

Supplementary Document for MATTopo: Topology-preserving Medial Axis Transform with Restricted Power Diagram

NINGNA WANG, University of Texas at Dallas, USA

HUI HUANG, Shenzhen University, China

SHIBO SONG, Independent Researcher, China

BIN WANG, Tsinghua University, China

WENPING WANG, Texas A&M University, USA

XIAOHU GUO*, University of Texas at Dallas, USA

CCS Concepts: • Computing methodologies → Shape analysis.

Additional Key Words and Phrases: Medial Axis Transform, Topology Preservation, Feature Preservation, Restricted Power Diagram

ACM Reference Format:

Ningna Wang, Hui Huang, Shibo Song, Bin Wang, Wenping Wang, and Xiaohu Guo. 2024. Supplementary Document for MATTopo: Topology-preserving Medial Axis Transform with Restricted Power Diagram. *ACM Trans. Graph.* 1, 1 (September 2024), 4 pages. <https://doi.org/10.1145/nnnnnnn.nnnnnnn>

1 IMPLEMENTATION DETAIL

Our code [is available at our project website](#), and the generated medial mesh can be viewed using the tool [blender-mat-addon](#) [Song and Wang 2023]. Our algorithm starts with a tetrahedral mesh $\mathcal{T} = \{\mathbf{t}_t\}_{t=1}^T$ and a set of medial spheres $\{\mathbf{m}_i\}_{i=1}^N$ as input, similar to Liu et al. [2020]. Each tet \mathbf{t}_t is a tetrahedral element represented by four ordered vertices, with indices 0, 1, 2, 3. And any combination of three vertices forms a triangle face of the tet. During each iteration, a set of new medial spheres $\{\mathbf{m}_j\}_{j=1}^M$ will be generated for preserving various medial axis properties. We only select a subset of tets from \mathcal{T} related to the new spheres $\{\mathbf{m}_j\}_{j=1}^M$ and compute the intersection among them. Thus, the RPD is updated partially instead of re-computing everything as a whole, for saving computational cost. Two important parameters used in our modified ‘Tet-Cell’ strategy [Liu et al. 2020] are:

- Sphere Neighbors (k_{site}): compute the k -nearest spheres to each sphere;
- Tet-Sphere Relations (k_{tet}): compute the k -nearest spheres to each tet.

*Corresponding author

Authors' addresses: Ningna Wang, University of Texas at Dallas, Texas, USA, ningna.wang@utdallas.edu; Hui Huang, Shenzhen University, Shenzhen, China, hhzhiyan@gmail.com; Shibo Song, Independent Researcher, Shanghai, China, longmaythess@outlook.com; Bin Wang, Tsinghua University, Beijing, China, wangbins@tsinghua.edu.cn; Wenping Wang, Texas A&M University, Texas, USA, wenping@tamu.edu; Xiaohu Guo, University of Texas at Dallas, Texas, USA, xguo@utdallas.edu.

Permission to make digital or hard copies of all or part of this work for personal or classroom use is granted without fee provided that copies are not made or distributed for profit or commercial advantage and that copies bear this notice and the full citation on the first page. Copyrights for components of this work owned by others than ACM must be honored. Abstracting with credit is permitted. To copy otherwise, or republish, to post on servers or to redistribute to lists, requires prior specific permission and/or a fee. Request permissions from permissions@acm.org.

© 2024 Association for Computing Machinery.

0730-0301/2024/9-ART \$15.00

<https://doi.org/10.1145/nnnnnnn.nnnnnnn>

When extending the Voronoi diagram to power diagram, the calculation of these two parameters also needs to be updated.

1.1 Sphere Neighbors

Changing the half-space equation from bisectors to radical hyperplanes implies that the ‘Security Radius’ criterion [Lévy and Bonneel 2013] used in [Ray et al. 2018] and [Liu et al. 2020] is not sufficient anymore to guarantee the correctness of the clipping. A sphere \mathbf{m}_i may have a neighboring sphere \mathbf{m}_j with larger radius much closer to \mathbf{m}_i in power distance than other spheres, while the center of \mathbf{m}_j is further to \mathbf{m}_i than others in Euclidean distance. To ensure the completeness of our algorithm during clipping process, we use the *Regular Triangulation* in CGAL [Fabri and Pion 2009] to pre-compute all possible neighbors $k_{neigh}(\mathbf{m}_i)$ of a given sphere \mathbf{m}_i .

1.2 Tet-Sphere Relations

Determining the number of possible spheres whose power cell has potential intersection with the given tet (k_{tet}) is an another key parameter for the proposed algorithm. Unfortunately, the heuristic estimation of k_{tet} proposed by Liu et al. [2020] is not reliable and requires fine-tuning for different models, as it is based on the ratio of the number of spheres to the number of tets. Brute-forcely traverse all possible combinations of tet and sphere is also a waste of computational resources. Hence, we propose an easy work-around implementation to filter the unrelated tet-sphere pairs as much as possible.

Given a tet \mathbf{t}_t and sphere \mathbf{m}_i , we want to decide whether \mathbf{t}_t has intersection with RPC $\omega_c(\mathbf{m}_i)$ potentially. We traverse all half-spaces $\Pi^+(\mathbf{m}_i, \mathbf{m}_j)$ defined by medial sphere \mathbf{m}_i and its neighboring sphere \mathbf{m}_j and maintains a counter d . If any vertex v of \mathbf{t}_t is closer to \mathbf{m}_i than \mathbf{m}_j measured under power distance, we increase the counter d by 1. This means v is on the positive side of half-space $\Pi^+(\mathbf{m}_i, \mathbf{m}_j)$. Taking Fig. 1 (a) as an example. For half-space $\Pi^+(\mathbf{m}_i, \mathbf{m}_{j_3})$, vertex v_1 is on the negative side, but v_2 and v_3 are on the positive side, so $d+1$ for this half-space. After traversing all half-spaces, we think tet \mathbf{t}_t is very likely to be related to sphere \mathbf{m}_i if the counter d equals to the number of neighboring spheres of \mathbf{m}_i . Hence in Fig. 1 (a) the tet \mathbf{t}_t is related to sphere \mathbf{m}_i , but in Fig. 1 (b) it does not. It is worth noting that this strategy only filters out most of the unrelated spheres for each tet, e.g., the number of related tets decreases from 4986 to 126 for model #9624 of $\#s = 138/3684$ set of medial spheres. However, it does not guarantee giving the minimum number of related spheres for each tet. Fig. 1 (c) shows an example where tet \mathbf{t}_t

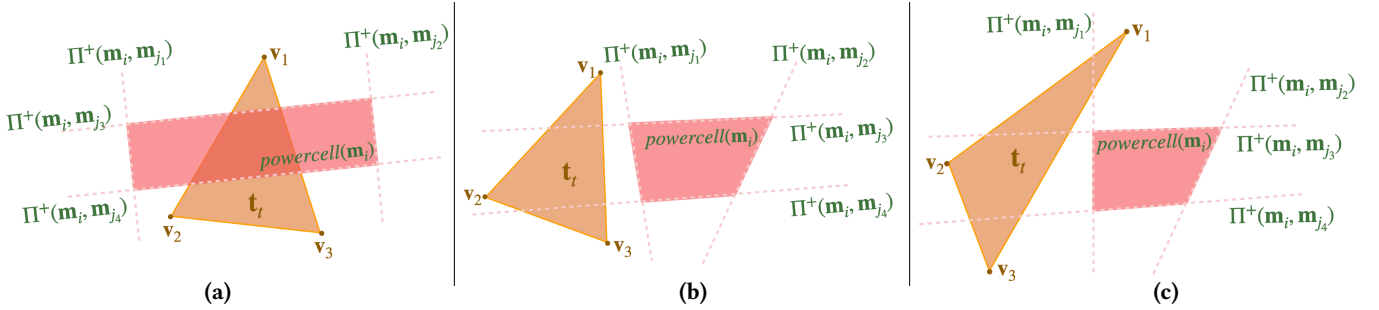


Fig. 1. 2D Illustration of ‘Tet-sphere’ relations described in Sec 1.2.

is considered relating to sphere m_i using proposed algorithm but it may not really intersect with the power cell of m_i . The pseudo-code is given in Alg. 1.

We compute this binary relation for every pair of tet-sphere. Each tet-sphere pair can be evaluated independently, thus suitable for GPU implementation. After extracting the spheres that return the positive result for each tet, we can count the number of related spheres per tet as the value of k_{tet} .

ALGORITHM 1: Determine whether tet t_t relates to sphere m_i

Data: medial sphere m_i , the set of neighboring spheres $k_{neigh}(m_i)$, and tet t_t

Result: Boolean whether tet t_t relates to sphere m_i

```

1  $d \leftarrow 0$  // stores the number of related half-spaces
2 for each sphere  $m_j \in k_{neigh}(m_i)$  do
3   for each vertex  $v$  of tet  $t_t$  do
4     if ( $\text{PowerDistance}(m_i, v) < \text{PowerDistance}(m_j, v)$ )  $d++$ ;
5     break;
6   end
7 end
8 if  $d == \text{len}(k_{neigh}(m_i))$  then
9   return True
10 end
11 return False

```

2 MORE RESULTS

Here we show more quantitative comparison results in Table 1, Table 2 and Table 3. We ran our method on the first 100 models in the ABC dataset [Koch et al. 2019] under the *10k/test* folder using 2048 as the number of mesh vertices. Here we filter these models using the same method as MATFP [Wang et al. 2022], as our method also only focuses on closed, manifold model with a single connected component and no self-intersection. We also ran the qualitative comparison on 14 organic models. All experiments are run on a computer with a 3.60GHz Intel(R) Core(TM) i7-9700K CPU and 32 GB memory.

We ran VC [Yan et al. 2018] using 2^8 as the voxel size and pruning parameter $\lambda = 0.03$. For SAT [Miklos et al. 2010], we use $\delta = 0.03$ and set the scale parameter as default 1.0. The geometric error bound δ^ϵ used in our method is set to 1.5.

We use the same evaluation metrics as the main paper (Sec.5), where ϵ^1 is the one-sided Hausdorff distance from the original

surface to the surface reconstructed from MAT, and ϵ^2 is the distance in reverse side. All Hausdorff distances are evaluated as percentages of the distance over the diagonal lengths of the models’ bounding box. The ϵ^{max} is the maximum of ϵ^1 and ϵ^2 . We mark the best error result ϵ^{max} as **bold** and the second best with underline in Table 1. We also show #s as the number of medial spheres for the medial meshes generated from each method, and mark the smallest number with superscript \star . We use the *Euler characteristics* X as the topology measures for the generated medial mesh, and show the ground truth Euler characteristic of the input shape as ‘GT X ’. The incorrect X is marked in red. Note that some results of VC may have Euler characteristic deviates from the GT X , e.g., model #2124 with GT $X = -8$ but VC computes $X = -17$. This might be because of two reasons: (1) the voxel size 2^8 is not dense enough for this model; (2) the pruning parameter $\lambda = 0.03$ is too big for it.

For PC, SAT, and VC, there are some models returning empty results using the current parameters, e.g., model #08145, where we leave them empty in Table 1. Fine tuning other parameters for these three methods may solve this problem. For some models whose tetrahedral mesh contains too many tets, our method would fail to compute the corresponding RPD thus no output is given. For example, model #12182 contains over 6 million tets even using the fTetwild [Hu et al. 2020] method with the largest length parameter value $l = 1$. We also leave these results empty in the table.

REFERENCES

- Andreas Fabri and Sylvain Pion. 2009. CGAL: The computational geometry algorithms library. In *Proceedings of the 17th ACM SIGSPATIAL international conference on advances in geographic information systems*. 538–539.
- Yixin Hu, Teseo Schneider, Bolun Wang, Denis Zorin, and Daniele Panozzo. 2020. Fast tetrahedral meshing in the wild. *ACM Transactions on Graphics (TOG)* 39, 4 (2020), 117–1.
- Sebastian Koch, Albert Matveev, Zhongshi Jiang, Francis Williams, Alexey Artemov, Evgeny Burnaev, Marc Alexa, Denis Zorin, and Daniele Panozzo. 2019. Abc: A big cad model dataset for geometric deep learning. In *Proceedings of the IEEE/CVF conference on computer vision and pattern recognition*. 9601–9611.
- Bruno Lévy and Nicolas Bonneel. 2013. Variational anisotropic surface meshing with Voronoi parallel linear enumeration. In *Proceedings of the 21st international meshing roundtable*. Springer, 349–366.
- Xiaohan Liu, Lei Ma, Jianwei Guo, and Dong-Ming Yan. 2020. Parallel computation of 3D clipped Voronoi diagrams. *IEEE Transactions on Visualization and Computer Graphics* 28, 2 (2020), 1363–1372.
- Balint Miklos, Joachim Giesen, and Mark Pauly. 2010. Discrete scale axis representations for 3D geometry. In *ACM SIGGRAPH 2010 papers*. 1–10.
- Nicolas Ray, Dmitry Sokolov, Sylvain Lefebvre, and Bruno Lévy. 2018. Meshless Voronoi on the GPU. *ACM Transactions on Graphics (TOG)* 37, 6 (2018), 1–12.
- Shibo Song and Ningna Wang. 2023. blender-mat-addon. <https://github.com/songshibo/blender-mat-addon>.

Table 1. Statistics of quantitative comparison results described in Sec 2.

Model ID (GT E)	PC				SAT				VC				MATTOP				Ours			
	#s	ϵ^1	ϵ^2	X	#s	ϵ^1	ϵ^2	X	#s	ϵ^1	ϵ^2	X	#s	ϵ^1	ϵ^2	X	#s	ϵ^1	ϵ^2	X
00549(-6)	29k	4.477	3.477	2k	45k	2.027	2.203	-33	86k	4.913	6.927	-6	21k	1.282	1.151	-5	7.2k*	0.787	1.077	-6
01188(-2)	4k	2.116	1.878	197	27k	0.833	3.652	3	33k	2.302	2.727	-2	9.9k	0.698	0.336	-2	1.4k*	0.617	1.494	-2
01510(-2)	10k	2.376	3.432	212	23k	1.584	2.324	13	79k	2.722	3.486	-2	7.7k	1.455	1.069	-2	3k*	0.699	1.371	-2
02000(0)	22k	2.477	1.58	23	31k	3.583	4.230	10	112k	1.556	2.917	0	7.4k	1.999	1.468	0	6.3*k	1.053	1.686	0
02124(-8)	18k	2.612	2.612	27	26k	2.565	1.565	-106	302k	1.578	1.002	-17	15k	0.486	0.52	-8	3.9k*	0.501	0.742	-8
02596(-4)	48k	1.234	2.102	20k	31k	1.503	2.098	-9	73k	1.987	1.703	-4	27k	1.363	0.955	-2	-	-	-	-
02995(1)	35k	3.138	2.138	333	32k	1.820	3.448	6	67k	2.715	2.106	1	19k	0.85	3.927	14	9.3k*	0.565	1.454	1
03774(-1)	9k	3.543	4.543	682	15k	1.907	3.907	73	41k	2.960	3.408	-1	27k	0.152	0.115	-1	3k*	0.512	0.972	-1
03829(0)	21k	2.341	1.234	15	31k	2.111	2.457	15	114k	1.665	1.942	0	11k	0.607	0.609	0	7.3k*	0.601	0.881	0
04123(-3)	16k	2.282	1.79	4	22k	1.659	2.209	-30	42k	5.553	9.098	-3	17k	0.78	3.799	-1	5.1k*	0.635	1.095	-3
05185(-1)	31	3.077	9.077	71	30k	2.200	3.404	29	279k	3.055	13.453	-1	8k	1.263	1.065	-1	4.8k*	1.414	1.484	-1
05227(-5)	19k	1.103	2.103	994	15k	4.612	2.612	-23	29k	1.858	2.583	-5	12k	0.442	0.338	5	3.2k*	0.532	1.419	-5
05302(0)	17k	2.099	1.099	20	-	-	-	-	54k	1.809	1.153	0	7k	0.279	0.281	0	2.5k*	0.613	0.613	0
07181(0)	12k	2.709	2.918	2k	17k	2.485	2.599	6	28k	1.748	1.423	0	5k	0.646	0.43	0	1.4k*	0.542	0.970	0
07446(0)	28k	2.618	3.618	4k	17k	1.794	2.652	11	15k	2.089	3.096	0	24k	0.817	0.621	0	6.1k*	0.715	1.209	-
07879(-1)	7k	1.672	1.672	12	11k	1.334	2.344	3	22k	1.672	1.109	-1	10k	0.364	0.324	-1	2.3k*	0.598	0.867	-1
08145(1)	17k	1.294	2.843	1k	-	-	-	-	-	-	-	-	25k	0.635	0.101	7	-	-	-	-
08315(-4)	19k	2.234	1.648	355	30k	1.540	2.864	11	95k	2.635	2.933	-4	11k	0.713	3.351	-2	1.5k*	1.481	1.132	-4
08812(1)	19k	2.249	1.249	705	37k	1.212	2.842	11	219k	1.617	1.904	-1	15k	0.728	0.563	1	9.6k*	1.476	1.356	1
08964(-72)	19k	1.765	1.765	5k	27k	0.874	0.874	71	-	-	-	-	25k	0.251	0.132	-37	8.7k*	0.685	0.753	-72
09624(-4)	22k	1.755	2.335	23	31k	2.180	2.590	11	157k	1.617	1.925	-4	6.8k	0.459	0.466	-4	3.7k*	0.666	0.954	-4
09796(-3)	24k	2.387	3.387	831	38k	1.584	2.584	-50	227k	0.789	1.470	-5	29k	0.384	0.344	-3	4k*	0.548	0.692	-3
10170(0)	11k	2.957	2.957	1.4k	23k	1.923	1.987	-7	116k	1.109	3.943	0	15k	0.982	2.013	0	3k*	0.589	0.842	0
10470(1)	19k	0.487	0.636	5k	14k	0.817	0.970	1	-	-	-	-	9.7k	0.21	0.277	1	2.5k*	0.529	0.580	1
10595(0)	-	-	-	-	22k	2.105	2.105	9	87k	1.896	2.701	0	5.6k	1.606	1.904	0	3k*	0.634	1.076	0
10721(1)	8k	1.023	2.412	18k	13k	0.950	1.446	25	24k	1.715	1.180	1	9k	0.479	0.312	1	2.5k*	0.424	0.678	1
10836(-1)	17k	1.81	2.309	3k	13k	1.195	2.016	7	46k	0.756	3.041	-1	3k	1.067	0.746	1	2.7k*	1.296	1.496	-1
11299(-24)	10k	1.066	1.247	1.7k	12k	2.550	2.550	-27	46k	2.470	2.749	-24	19k	0.37	2.324	-13	5.8k*	0.533	0.961	-24
11368(0)	-	-	-	-	31k	1.323	2.566	39	94k	1.921	2.974	0	11k	1.067	0.583	0	4.8k*	0.811	1.448	0
11476(-2)	15k	1.29	0.292	211	23k	1.296	2.911	7	41k	2.725	2.183	-2	9k	0.873	0.497	-2	3.5k*	0.597	0.803	-2
11507(-5)	12k	1.04	3.477	342	28k	1.457	4.170	-41	58k	1.028	2.833	-5	16k	0.996	0.622	-5	7.4k*	0.713	0.948	-5
11527(-6)	29k	1.384	0.334	1.1k	12k	1.238	1.341	-35	19k	0.624	0.986	-6	12k	0.256	0.176	-6	2.1k*	0.416	0.863	-6
11628(-18)	14k	2.664	2.112	130	40k	1.278	1.504	2	30k	0.441	6.709	-18	31k	0.184	0.112	-	5.6k*	0.486	0.717	-18
11790(0)	15k	1.393	2.833	32	25k	1.207	2.659	8	72k	1.790	1.066	0	17k	1.79	1.319	2	5.3k*	0.764	0.819	0
11800(1)	13k	1.56	0.36	32	19k	3.322	4.322	6	18k	1.696	1.024	1	8k	0.28	0.253	1	2.3k*	0.431	0.522	1
11835(0)	23k	0.763	2.533	2k	25k	1.371	2.814	-54	36k	2.970	2.615	0	21k	1.032	2.252	-16	5.4k*	0.545	1.015	0
12047(1)	5k	2.393	3.205	15k	23k	1.281	1.974	10	77k	2.677	2.177	1	5k	2.47	1.592	1	3k*	1.235	1.487	1
12182(1)	-	-	-	-	-	-	-	-	60k	1.663	2.148	1	9.6k*	1.125	0.818	1	-	-	-	-
12254(-2)	9k	1.13	2.31	81	19k	3.513	4.027	-11	59k	3.076	4.076	-2	19k	0.915	0.507	-2	4.5k*	0.816	1.254	-2
12261(0)	21k	1.012	2.439	3k	4k	1.199	3.311	4	17k	2.096	2.830	0	3k	0.313	0.252	0	3.7k*	1.246	1.453	0
12280(1)	-	-	-	-	-	-	-	-	26k	3.998	2.446	1	8k*	2.503	0.501	1	-	-	-	-
12547(1)	15k	2.594	2.594	149	24k	2.426	3.790	12	57k	2.661	3.720	1	9.9k	1.991	1.606	1	4.2k*	1.196	1.426	1
12618(-16)	16k	2.531	1.523	2k	-	-	-	-	-	-	-	-	38k*	0.673	1.922	-28	-	-	-	-
12621(-3)	12k	2.391	1.299	31k	21k	3.698	3.464	-10	41k	3.172	5.317	-3	13k	1.19	0.788	-3	3.8k*	0.896	1.151	-3
12642(-12)	11k	0.453	1.293	485	13k	1.476	1.769	-7	74k	6.395	6.795	-237	17k	0.596	0.471	-12	4.3k*	0.567	0.809	-12
12749(1)	23k	2.355	2.324	181	23k	2.661	2.661	-30	139k	1.583	0.963	1	11k	0.764	0.865	1	5.3k*	0.376	0.467	1
12995(-3)	12k	2.254	1.254	449	24k	1.476	1.670	14	38k	1.899	1.497	-3	8k	0.804	0.657	-3	2.2k*	0.700	1.045	-3
13014(1)	2k	1.294	2.843	4k	15k	4.897	3.238	24	24k	1.795	1.154	1	7k	0.243	0.179	1	1k*	0.735	0.735	1
13026(-4)	40k	2.495	1.493	76k	40k	3.217	2.512	-167	226k	1.518	2.270	-4	26k	2.203	0.698	-2	10k*	0.715	1.241	-4
13151(0)	14k	1.948	2.451	18k	15k	3.652	2.034	62	44k	2.556	1.939	0	23k	0.519	0.495	0	3.2k*	0.604	0.902	0
13607(-13)	28k	1.294	0.289	2.9k	27k	1.809	1.809	-17	65k	1.324	8.380	-13	19k	0.956	0.376	-19	7.3k*	1.486	0.896	-13
13624(1)	14k	0.765	1.81	138	18k	0.897	1.879	-63	-	-	-	-	17k	0.665	0.548	1	3.6k*	0.651	1.301	1
13652(1)	43k	1.725	1.145	1.6k	-	-	-	-	19k	7.877	8.683	1	23k*	1.466	0.666	1	-	-	-	-
13952(-1)	7k	2.481	1.293	68	39k	1.377	2.904	60	115k	1.674	2.244	-1	13k	1.095	0.78	-1	2.4k*	0.928	0.998	-1
14326(-2)	28k	1.165	2.13	1k	31k	2.281	2.806	1	73k	4.383	6.668	-2	24k							

Table 2. Statistics of quantitative comparison results described in Sec 2.

Model (GT E)	PC				SAT				VC				MATFP				Ours			
	#s	ϵ^1	ϵ^2	X	#s	ϵ^1	ϵ^2	X	#s	ϵ^1	ϵ^2	X	#s	ϵ^1	ϵ^2	X	#s	ϵ^1	ϵ^2	X
15288(0)	10k	2.34	1.143	26	12k	2.026	2.577	-8	49k	<u>1.549</u>	1.443	-	17k	0.244	2.142	0	1.8k*	0.445	0.784	0
15807(-1)	39k	4.295	4.583	499	25k	1.537	2.018	5	16k	1.068	3.602	-1	11k	<u>1.183</u>	0.938	-1	4.6k*	0.626	1.276	-1
15875(-1)	8k	1.581	1.321	2k	12k	1.557	2.723	3	16k	1.597	2.485	-1	7k	0.624	0.435	0	2.5k*	0.506	<u>0.932</u>	-1
16150(1)	13k	0.872	2.432	3k	-	-	-	-	54k	1.507	1.267	1	3k	0.899	<u>1.045</u>	1	1k*	0.452	0.901	1
16489(-2)	-	-	-	-	24k	2.127	2.133	17	55k	0.729	1.124	-2	15k	<u>0.719</u>	0.657	-2	4.6k*	0.459	0.593	-2
17061(-4)	21k	2.194	3.431	775	43k	1.849	2.097	0	243k	<u>1.676</u>	1.099	-4	17k	1.933	1.468	-29	6.1k*	0.905	1.414	-4
17150(1)	25k	3.087	2.491	2k	22k	2.569	2.643	1	52k	1.130	2.280	1	16k	<u>1.231</u>	0.797	1	5.3k*	0.716	1.205	1

Table 3. Statistic of quantitative comparison results on organic models.

Model (GT E)	PC				SAT				VC				MATFP				Ours			
	#s	ϵ^1	ϵ^2	X	#s	ϵ^1	ϵ^2	X	#s	ϵ^1	ϵ^2	X	#s	ϵ^1	ϵ^2	X	#s	ϵ^1	ϵ^2	X
Armadillo(1)	13k	1.455	1.109	58	16k	1.402	1.280	5	31k	3.693	1.218	1	24k	<u>1.201</u>	0.733	47	8k*	1.020	0.825	1
Bear(1)	18k	0.346	<u>0.412</u>	6	14k	0.736	0.723	7	22k	0.535	0.511	1	5k	<u>0.346</u>	0.402	1	2k*	0.510	0.512	1
Buddha(-7)	20k	<u>1.685</u>	1.139	88	26k	2.254	1.377	11	28k	4.604	1.388	-	-	-	-	-	10k*	1.157	1.018	-7
Bug(1)	11k	0.527	0.442	1.2k	9k	1.196	4.259	18	14k	1.369	1.120	1	7k	0.288	0.253	4	3k*	<u>0.459</u>	0.436	1
Chair(-2)	11k	2.466	2.626	75	10k	0.727	0.761	26	25k	0.608	0.562	-2	7k	<u>0.322</u>	0.344	-2	3k*	<u>0.542</u>	0.509	-2
Dolphin(1)	5k	0.756	0.691	257	10k	0.933	1.873	15	15k	5.611	1.369	1	4k	0.333	<u>0.356</u>	1	1k*	0.859	0.949	1
Fertility(-3)	14k	1.885	1.822	557	17k	2.142	2.623	11	36k	2.4132	2.373	-3	11k	1.014	<u>1.028</u>	-1	5k*	0.453	0.411	-3
Hand(1)	7k	2.854	6.192	114	11k	1.014	2.623	4	27k	0.496	0.724	1	6k	0.378	0.349	1	2k*	0.503	<u>0.519</u>	1
Plane(1)	5k	1.041	1.109	351	6k	0.917	0.987	3	12k	3.296	1.269	1	5k	0.282	0.228	1	2k*	0.814	<u>0.849</u>	1
Pig(1)	8k	<u>1.351</u>	0.653	351	13k	1.18188	3.412	16	18k	1.223	1.394	1	-	-	-	-	4k*	0.889	0.802	1
Rozy(1)	13k	1.459	1.574	513	23k	1.196	1.287	7	39k	2.023	1.101	1	22k	<u>1.264</u>	1.106	4	9k*	0.933	0.831	1
Spider(1)	12k	0.592	<u>0.690</u>	83	8k	1.031	3.825	32	20k	5.661	0.978	1	7k	0.255	0.247	1	4k*	0.818	0.759	1
Teapot(-4)	15k	1.763	0.745	463	18k	2.568	1.573	3	27k	<u>1.689</u>	1.673	-4	11k	1.912	1.019	-8	4k*	1.063	0.664	-4
Venus(1)	7k	1.098	0.979	21	16k	<u>1.490</u>	1.428	27	22k	2.929	2.434	1	2k	1.645	1.436	1	3k*	1.149	0.991	1

Ningna Wang, Bin Wang, Wenping Wang, and Xiaohu Guo. 2022. Computing Medial Axis Transform with Feature Preservation via Restricted Power Diagram. *ACM Transactions on Graphics (Proceedings of SIGGRAPH Asia 2022)* 41, 6 (2022).

Yajie Yan, David Letscher, and Tao Ju. 2018. Voxel cores: Efficient, robust, and provably good approximation of 3d medial axes. *ACM Transactions on Graphics (TOG)* 37, 4 (2018), 1–13.